

# Nanostructured Materials for Effective Electromagnetic Interference Shielding Applications – A Review

NasreenTaj M<sup>1</sup>, Daruka Prasad B<sup>2,a</sup>, N Rama Rao<sup>3</sup>, NagabhushanaH<sup>4,b</sup>

<sup>1</sup>Department of Electrical and Electronics Engineering, HMS Institute of Technology, Tumakuru-572104, India

<sup>2</sup>Department of Physics, BMS Institute of Technology and Management, Avalahalli, Bangalore-560064, India

<sup>3</sup>Department of Electrical and Electronics Engineering, BMS Institute of Technology and Management, Bangalore-560064, India

<sup>4</sup>Prof. C.N.R. Rao Centre for Advanced Materials Research, Tumkur University, Tumakuru-572 103, India

## Abstract:

In the present review, the nanomaterials, composites synthesized by different methods which can be effectively used as shielding materials for electromagnetic radiations interference in the X-band range. This review article covers different aspects of nanoscience developed and its scope for further studying the different properties and establishing different shielding materials for Electromagnetic Interference shielding. It provides the comprehensive details of the MXane, carbon, graphene, polymer composites based materials performance for the shielding application in the frequency range of 8 GHz to 12 GHz. Also reviewed based on the thickness and also the morphology how the shielding was able to tune and can be used for various fields of applications.

**Keywords:** Nano materials, Electromagnetic Interference shielding (EMI), Composites, Polymers.

## 1. INTRODUCTION

### 1.1 Electromagnetic Interference (EMI) shielding

It was observed that recently there was an increased miniaturization of the electronic devices which enhances the heat production and also noise known as electromagnetic interference (EMI) of signals. These effects decline the permanence and operation of electronic devices such as cell phones, computers, blue tooth devices, laptops, microwave ovens etc. These Electromagnetic (EM) wave radiations scaled up from the range of megahertz (MHz) to gigahertz (GHz) scatters to the fields of communication, medical diagnostics and to the renewable energy applications [1-3]. Hence, to enhance the performance of these devices, there

was a need of controlling the interference of signals and also absorb the heat produced locally. This can be achieved by using different conducting and non-conducting materials as shielding to these EM radiations [4].

Increased EM wave's usage for various applications led to impact of them on the human health and environment. These waves affect the normal functioning of the electronic devices in the systems which were sensitive to operation viz., aerospace, control systems and antenna applications [5]. Usually metal based materials were used for the Electromagnetic shielding (EMS). Use of metals for EMS, produce radiation pollution due to emission of secondary radiations, their density adds excess weight and they easily corrode to harsh environment. Till date the preferred metals used were composites of metals such as silver, copper, nickel, aluminum and metalized plastics. These conductive composites have drawbacks such as brittleness, low impact resistance, high density, galvanic corrosion for the metal composites [6, 7]. But recently, polymer-based EMI shielding composites (PEMI) showed better EMS performance which were studied by the scientific and industrial communities [8, 9]. PEMI have advantages such as lighter, more specific strength, easy to prepare, stable chemically and low cost when compared to metal based EMI materials

Polymers show non-conducting nature, hence they don't allow electric charges to move which leads to poor EMS [10, 11]. Introducing conductive fillers such as carbon/metal fibers and carbon nanotubes (CNTs) into these will help to increase electrical conductivity and EMS properties. Various polymer matrices allow the impurities/dopants to trap in their complex molecular matrix and changes their electrical properties significantly which helps for the EMI shielding [12-14]

Commonly used polymers were epoxy/resins, polyvinylidene fluoride (PVDF) and polydimethylsiloxane (PDMS). PDMS was mostly used polymer in many fields such as aerospace, automobile and micro/nanoelectronic industries and it provides better flexibility to devices making. This was because it has

more stable, good mechanical properties, good temperature resistance, non-reactive to the climatic and chemical changes and easy processing. There was a need of development of polymer based EMS materials which have low filler loading which helps in obtaining the desired EMS effectiveness where the high filler loading with low cost was possible [15-17].

EMS was defined as reflection and/or absorption of EMR by a material that acts as an obstacle for the penetration of the radiation passing through the shielding materials (SE). EMS can be achieved by high reflecting materials such as conductors or by high permeable materials such as magnetic materials. But magnetic materials lose their magnetic properties within GHz range due to intrinsic cutoff frequency. Presently, there was a requirement to investigate larger bandwidth shielding materials; which prevent / neutralize EM waves in the MHz to GHz range. Literature shows many reports which explained the various approaches to achieve this but still there was a scope for simultaneously reducing the reflection and enhancing the absorption was still requires some more approaches /new techniques for practical applications [3, 18-20].

$$\delta = -8.68 \left( \frac{t}{SE_A} \right) \quad \dots(1)$$

## 1.2 Nanomaterials

Nano particles (NPs) were those whose dimensions must be in the range of 100 nm in at least one of its dimensions. Nowadays much attention has been focused on metals, metal oxides and other compositions in nano-regime as their properties may significantly differ from their respective bulk. NPs surface area to volume ratio increases significantly compared to its bulk counterpart makes the materials active due to the increased exposure of atoms/ions/molecules to the surrounding environment. Quantum confinement effect

was additional phenomena which make these materials special in terms of their energy band gap, charge transport properties and other mechanical, optical and electrical properties. Silicates were minerals containing silicon and oxygen in tetrahedral units which can be linked together in different patterns and silicates exists on the Earth's crust enormously. It exists in different forms based on tetrahedral unit links such as ortho, pyro, cyclic, chain, sheet etc. Among them ortho silicate was more common. Strontium was a divalent silvery metal which was harder than barium and softer than calcium. It was a good absorber of X-rays, biocompatible, provide glow to the paints. Silicates in nano-regime have showed the better material for electronics and medical fields due to their bio-compatibility, stability, and easily get functionalized with other molecules / polymers.

## 2. EMI shielding Process and Mechanisms

### 2.1.1 Shielding efficiency in terms of reflection/absorption.

SE was the parameter which measures the quantity of EM energy of particular frequency which was hindered by the material when it was propagated through it. Fig. 1a shows the schematic representation of EM waves interactions with matter. Inside the material, sources of reflections, absorptions and multiple reflections were showed when it has thin or thick size and various surface structures. Incident power ( $P_I$ ) dissipated through the material in terms of reflection ( $P_R$ ) or multiple reflections, absorption ( $P_A$ ), and the remaining part gets transmitted ( $P_T$ ) through the shielding material. Corresponding attenuations can be named as  $SE_T$  which was due to  $SE_R$ ,  $SE_A$  and  $SE_M$ , respectively.

$$SE_T = 10 \log \frac{P_I}{P_T} = 20 \log \frac{E_I}{E_T} = 20 \log \frac{H_I}{H_T} = SE_R + SE_A + SE_M. \quad \dots\dots(2)$$

Here P, E and H refer to power, electric and magnetic field intensities and subscripts I, R and T represent the incident, reflected and transmitted components, respectively. Absorption occurs due to the molecular properties of the host and doped particles. Reflection generally occurs when the size of the particle matches with the wavelength of the incident waves and multiple reflections occurs due to the small potential flaws within the molecular gaps.

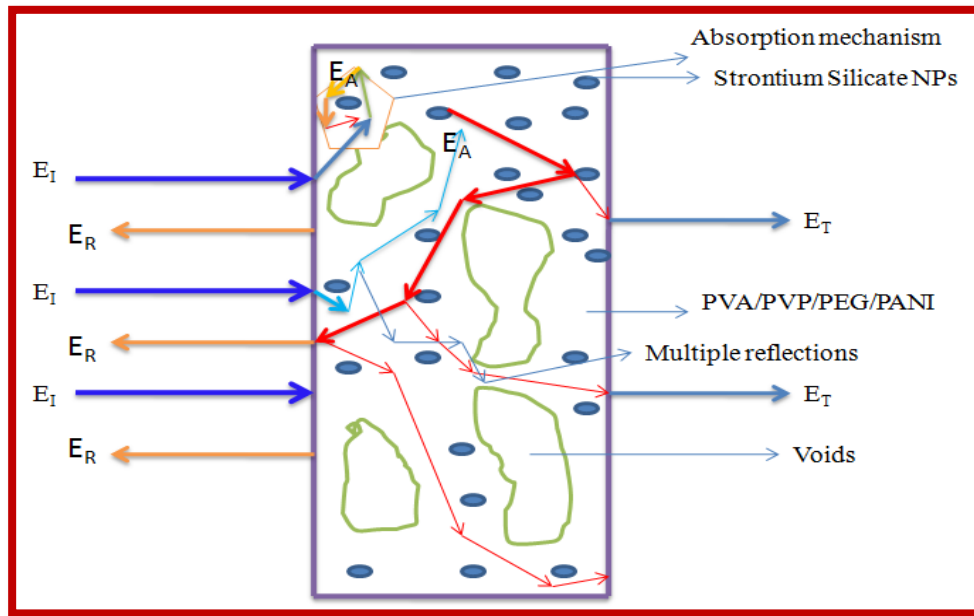


Fig.1: Mechanism of various phenomena associated with EMI shielding in a material.

### 2.1.2 Reflection loss ( $SE_R$ )

The primary mechanism of EMS was reflection.  $SE_R$  was due to the relative impedance mismatching between the particles size and the wavelength of EM waves as given below

$$SE_R = 20 \log \frac{Z_0}{4Z_{in}} = 39.5 + 10 \log \frac{\sigma}{2\nu\pi\mu} \quad \dots(3)$$

Where  $Z_0$  ; output impedance,  $Z_{in}$  ; input impedance,  $\sigma$  ; conductivity,  $\nu$  ; frequency, and  $\mu$ ; relative permeability. Materials should have free charge carriers (electrons or holes) for reflection of the EM waves hence SER decreases with  $\nu$ .

### 2.1.3 Absorption loss ( $SE_A$ ).

A secondary loss mechanism of EMS was absorption loss which results due to heating and eddy current loss. For conductive materials,  $SE_A$  in dB can be written as

$$SE_A = 20 \log e^{\frac{d}{\sigma}} = 8.7d\sqrt{\nu\pi\mu} \quad \dots\dots(4)$$

Where  $d$  ; thickness of the slab,  $\sigma$  ; conductivity,  $\nu$  ; frequency and  $\mu$  ; permeability of the material. Attenuation constant ' $\alpha$ ' was given by

$$\alpha = \frac{4\pi n}{\lambda_0} \quad \dots\dots(5)$$

Where  $\lambda_0$  was the wavelength in vacuum and  $n$  was the refractive index, which was given by  $(\epsilon\mu)^{1/2}$ ; in the case of nonmagnetic materials  $\mu=1$ . Hence,

$$\alpha = \frac{4\pi\epsilon^{1/2}}{\lambda_0} \quad \dots\dots(6)$$

It was clear from eqns (5) and (6) that high permittivity was particularly crucial for the enhancement of  $SE_A$ , as well  $S_R$ .

### 2.1.4 Shielding effectiveness due to Multiple reflections ( $SE_M$ ).

For material of thin size, radiation gets trapped between the boundaries due to multiple internal reflections as shown in Fig. 1a.

$$SE_M = 20 \log \left( 1 - e^{-\frac{2d}{\delta}} \right) \quad \dots\dots(7)$$

where  $\delta$ ; skin depth, defined as the thickness below them outer surface at which the incident field was attenuated to  $1/e$  of its initial value, given by

$$\delta = (f\pi\sigma\mu)^{-1/2} \quad \dots(8)$$

Multiple reflections take part in major role for porous structures and for well defined structures. Fig. 1 shows trapping/scattering of EM radiation by porous, hollow, multi-shell and solid structures. In this structure, scattering and multiple reflections of EM waves occurs due to a large surface area and a void space. The hollow/ porous structure shows properties such as high surface area, defects in the internal structures, and permeability which were responsible for x improving EMI mechanism. These multiple reflections ( $SE_M$ ) can be neglected when the thickness of the shielding materials was greater than the penetration depth ( $\delta$ ) or when  $SE_A$  was more than 10 dB.

### 2.1.5 Perspective to minimize reflection.

It is well known that in non-magnetic materials shielding was mainly governed by reflection, while in magnetic conducting metals, shielding was dominated by absorption rather than reflection. In the case of composite materials, presence of heterogeneous micro/nano structures which acts as polarization sites shows the variations in the local fields. These sites create the lag of the displacement current relative to conduction current. Further, a matrix and filler inclusion alters the EM properties. In these conditions, permittivity and permeability changes to complex forms as given below:

$$\varepsilon = \varepsilon' + j\varepsilon'' \quad \dots(9)$$

$$\mu = \mu' + j\mu'' \quad \dots(10)$$

where  $j$  was an imaginary number,  $\epsilon'$  and  $\mu'$  denotes the electric and magnetic energy storage capacities, while  $\epsilon''$  was related to dielectric losses and  $\mu''$  relates to Ohmic losses. Complex terms dependency is on the geometry, size, conductivity and volume fraction of each constituent. For several applications, the essential requirement was to adjust the effective permittivity and permeability values by which reflection can be minimized. Therefore, a prerequisite of conductive EMS composites was to limit reflection and enhance absorption. This was possible only when the mismatch of impedance between free space and shielding materials was minimized. According to the transmission line theory, intrinsic surface impedance for a given medium can be written as,

$$Z_{in} = \frac{|E|}{|H|} = \sqrt{\frac{fj2\pi\mu}{\sigma + fj2\pi\epsilon}} \quad \dots\dots\dots(11)$$

The microwave absorption properties of these materials in terms of reflection loss could be given by

$$R_L(\text{dB}) = 20 \log \left| \frac{Z_{in} - Z_0}{Z_{in} + Z_0} \right| \quad \dots\dots\dots (12)$$

The maximum absorption of microwaves means that a minimum reflection loss ( $RL_{\min}$ ) occurs when the impedance of the composite and free space was matched. The ideal impedance matching conditions were when  $Z_{in} = Z_0 = 377 \Omega$ . Here  $Z_0$  was the impedance of air,  $Z_{in}$  was the input impedance of the absorber. The above condition was fulfilled at a specific matching thickness ( $t_m$ ) and matching frequency ( $f_m$ ). An ideal EM absorption should make the effective width as broad as possible, which can be controlled by the  $1/4$  wavelength.

$$t_m = \frac{nc}{4f_m \sqrt{\epsilon\mu}} \quad \dots\dots\dots (13)$$

where  $n$  ; the refractive index and  $c$  ; the velocity of light. The RL value of -20 dB was considered to be 99% microwave absorption according to equations (8) and (11) for the adequate level of absorption. In order to

minimize the impedance mismatch, the best way was to increase the effective permeability or decrease the effective permittivity. Hence, high performance microwave absorbing materials have been considered extensively to prevent incident EM wave radiation. These materials convert EM energy into thermal energy through dielectric loss and/or magnetic loss by the balance outcome of integralities between the relative permittivity and/or permeability. Moreover, technological fields desire not only efficient shielders, but also they must fulfill some necessity criteria such as being lightweight, having a minimum, thickness, corrosion and chemical resistance, good flexibility, tunable morphology, ease of processing and cheaper.

## 2.2 Factors affecting the EMI performance

### 2.1.5 Perspective to minimize reflection.

In the case of non-magnetic materials, shielding was mainly governed by reflection. Further, in the composite materials, polarization sites lead to the permittivity variation which lags the flow of displacement current relative to conduction current. Further, a matrix and filler inclusion alters the EM properties. Variation of permittivity and permeability changes were represented as below:

$$\varepsilon = \varepsilon' + j\varepsilon'' \quad \dots\dots(9)$$

$$\mu = \mu' + j\mu'' \quad \dots\dots(10)$$

where  $j$ ; an imaginary number,  $\varepsilon'$  and  $\mu'$ ; the electric and magnetic energy storage capacities, while  $\varepsilon''$ ; to dielectric losses and  $\mu''$ ; Ohmic losses. Complex terms dependency is on the geometry, size, conductivity and volume fraction of each constituent. Adjusting the effective permittivity and permeability values by which reflection can be minimized is the minimum criteria which need to satisfied. Therefore, a prerequisite of conductive EMS composites was to limit reflection and enhance absorption. This was possible only when the

mismatch impedance between free space and shielding materials was kept minimum. According to the transmission line theory, intrinsic surface impedance for a given medium can be written as,

$$Z_{in} = \frac{|E|}{[H]} = \sqrt{\frac{fj2\pi\mu}{\sigma + fj2\pi\epsilon}} \quad \dots\dots\dots(11)$$

The microwave absorption properties of these materials in terms of reflection loss could be given by

$$R_L(\text{dB}) = 20 \log \left| \frac{Z_{in} - Z_0}{Z_{in} + Z_0} \right| \quad \dots\dots\dots (12)$$

The maximum absorption of microwaves means that a minimum reflection loss ( $RL_{\min}$ ) occurs when the impedance of the composite and free space was matched. The ideal impedance matching conditions were when  $Z_{in} = Z_0 = 377 \Omega$ . Here  $Z_0$  was the impedance of air,  $Z_{in}$  was the input impedance of the absorber. The above condition was fulfilled at a specific matching thickness ( $t_m$ ) and matching frequency ( $f_m$ ). An ideal EM absorption should make the effective width as broad as possible, which can be controlled by the 1/4 wavelength.

$$t_m = \frac{nc}{4f_m \sqrt{\epsilon\mu}} \quad \dots\dots\dots (13)$$

where  $n$  ; the refractive index and  $c$  ; the velocity of light. In order to minimize the impedance mismatch, the best way was to increase the effective permeability or decrease the effective permittivity. Hence, high performance microwave absorbing materials have been considered extensively to prevent incident EM wave radiation. These materials convert EM energy into thermal energy through dielectric loss and/or magnetic loss by the balance outcome of integralities between the relative permittivity and/or permeability. Moreover, technological fields desire not only efficient shielders, but also they must fulfill necessity criteria such as lightweight, minimum, thickness, corrosion, chemical resistance, good flexibility, tunable morphology, ease of processing and cheaper.

## 2.2 Factors affecting the EMI performance

**2.2.1 Permittivity and permeability.** Ideal EMS require impedance matching characteristics of composites which were influenced by  $\mu$  and  $\epsilon$

$$\alpha = \pi f c \sqrt{2(\mu''\epsilon'' - \mu'\epsilon' + \sqrt{(\mu'^2 + \mu''^2)(\epsilon'^2 + \epsilon''^2)}} \quad \dots(14)$$

For electrical shielding, conductivity and polarization losses were two key factors. Based on free electron theory, the presence of defects and residual groups in the material enhances the electric conductivity and it is possible at higher frequency regime. In this case, the relaxation process can be investigated by a Cole–Cole semicircle obtained from the Debye’s dipolar relaxation process [21]. The relationship between  $\epsilon'$  and  $\epsilon''$  is

$$(\epsilon' - \epsilon_\infty)^2 + (\epsilon'')^2 = (\epsilon_\delta - \epsilon_\infty)^2 \quad \dots(15)$$

where  $\epsilon_\delta$  and  $\epsilon_\infty$ ; the static and relative dielectric permittivity at higher frequencies. The anisotropy field  $H_a$  was given by  $H_a = 2K/\mu_0 M_s$ , where  $K$  was the anisotropy constant and  $M_s$  was the saturation magnetization, hence, smaller anisotropy field improves the absorption bandwidth.

### 2.2.4 Influential parameters for the EMS: -

**(a) Temperature and conductivity:** - Heat treatment creates defects in the form of vacancies, dangling bonds or substitutions in materials, these defects create an extra energy level around the Fermi level and hence enhance attenuation rather than reflection. Generally, the electrical properties of any of material shows better performance when the conductivity value is within the percolation threshold given by

$$\sigma = \sigma_0 (V - V_c)^c \quad \dots(16)$$

where  $\sigma$  ; the electrical conductivity of the materials,  $\sigma_0$  ; natural conductivity,  $V$  ; the volume fraction of filler,  $V_c$  ; the volume fraction at the percolation threshold and  $c$  ; the critical exponent. Depending on the shape, morphology, aspect ratio, distribution, concentration and compatibility of the filler with the host matrix etc., the percolation threshold value changes.

### (b) Thickness of the shielding material

The minimal reflection,  $RL_{\min}$  of the microwave power occurs when the thickness ‘t’ of the absorber is depending on the quarter integral multiple of the propagating wavelength

$$t_m = \frac{n\lambda_m}{4} \quad \dots(17)$$

where  $n = (1, 3, 5, 7, 9)$ , so that  $n = 1$  corresponds to the first dip at low frequency. The propagating wavelength in the material ( $\lambda_m$ ) was given by

$$\lambda_m = \frac{\lambda_0}{\sqrt{\mu\epsilon}} \quad \dots(18)$$

The matching condition results in the cancellation of the incident and rejected waves at the surface of the absorber material, Hence, with increasing sample thickness, reflection peaks shift toward the lower frequencies. Du et al. have shown the influence of shell thickness on the absorption properties of  $Fe_3O_4@C$  composites. A critical thickness of carbon shells shows superior dielectric behavior [22].

### 3. Measurement techniques

Experimentally, network analyzer instruments were used to measure EMS efficiency. There were two types of network analyzer: scalar network analyzers (SNA) and vector network analyzers (VNA). VNA has two ports ( $S_1, S_2$ ) indicates the incident and transmitted waves in terms of complex scattering (S) parameters, i.e.  $S_{11}$  or  $S_{22}$  and  $S_{21}$  or  $S_{12}$  respectively. These were known as the forward reflection coefficient ( $S_{11}$ ), the reverse

reflection coefficient ( $S_{22}$ ), the forward transmission coefficient ( $S_{12}$ ) and the backward transmission coefficient ( $S_{21}$ ). Different conversion approaches such as the short circuit line (SCL), NIST iterative, delta-function method, new non-iterative, transmission line theory and Nicolson–Ross– Weir (NRW) techniques have been adopted to obtain the characteristic parameters (i.e.  $\epsilon$ ,  $\mu$ ,  $R_L$  and  $Z$ ). Each method have their own limitations, SCL method can estimate  $\epsilon$  only, while the NIST iterative approach provides both  $\epsilon$  and  $\mu$  but with the limitation  $\mu=1$ . Parameters  $Z$  ( $\Omega$ ),  $RL$  (dB),  $SE_A$  (dB),  $SE_T$  (dB) and  $SE_R$  (dB) can be written as below:

$$Z=Z_0\left[\frac{1+S_{11}}{1-S_{11}}\right] \quad \dots(19)$$

$$RL=20\log|S_{11}| \quad \dots(20)$$

$$SE_T(\text{db})=10\log\left(\frac{1}{S_{12}^2}\right) = 10\log\left(\frac{1}{S_{21}^2}\right)=10\log\left(\frac{1}{T}\right) \quad \dots(21)$$

Where T was the transmittance

$$SE_R=10\log\left(\frac{1}{1-S_{11}^2}\right) = 10\log\left(\frac{1}{1-S_{22}^2}\right)=10\log\left(\frac{1}{(1-R)}\right) \quad \dots(22)$$

Where was R is the reflectance

$$SE_A =10\log\left(\frac{1-S_{11}^2}{S_{12}^2}\right) =10\log\left(\frac{1-S_{22}^2}{S_{21}^2}\right) = 10\log\left(\frac{1-R}{T}\right) \quad \dots(23)$$

Summation of the reflectance (R), transmittance (T) and absorbance (A) was always equal to 1

$$\text{i.e.,} \quad R + T + A=1 \quad \dots(24)$$

#### 4. Materials used for EMS

Various materials used for EMS were thin sheet of metals, CPs, NCPs, elastomers, carbon nanotubes, thin film nano-structured materials etc. They have the advantages such as light weight, easy synthesis processes, good environmental stability and dielectric loss properties make it a promising microwave absorbing material.

## Conducting polymers (CP)

In comparison to conventional metals and semiconductors, CPs possess exclusive properties such as a small density in the range of 1–1.3 g cm<sup>-3</sup> which is very less compared to metals. Structural flexibility along with the tunable conductivity in the range of 0.1–10<sup>-10</sup> S cm<sup>-1</sup>. CPs can be used in sensing, coatings and energy storage devices and microwave absorption applications. CPs were either prepared by electrochemical Oxidative Polymerization (EOP) or by the Chemical Oxidative Polymerization (COP) methods. The polymerization takes place by any of these approaches heat/radiation, the diffusion of the appropriate initiator, and then the organic initiator/catalyst was set on the surface of the NPs under the required temperature, pressure and stimulation conditions. In fact, fabrication of polymer nanocomposites (PNCs) was a hybridization process between the organic/inorganic PM and the inorganic/organic nanofillers to a single material which comprises integrated properties with respect to the matrix and filler only. This method also helps the modulation of shell thickness in the case of a core–shell structure just by controlling the weight ratio of the monomer, which influences the EM wave absorption properties effectively. According to dissipation mechanisms, microwave absorbing materials show dielectric loss and magnetic loss. In microwave absorbing materials, CPs serves as dielectric loss materials. Among the various conducting polymers, polyaniline (PANI), polypyrrole (PPy), poly(3,4-ethylenedioxythiophene) (PEDOT), polythiophene (PT), polyfuran (PF), poly(para-phenylene) (PPP) and poly(phenylenevinylene) (PPV) were of particular interest due to their easy availability, environmental sustainability, cost effectiveness and versatile doping chemistry.

### **Polyaniline (PANI) polymer**

Among the different CPs, polyaniline (PANI) was one of the most commonly used polymers as a host material for micro/nano-sized nanofillers owing to its unique physicochemical properties. These polymers show improved tensile strength and elongation at break, thermal stability and particularly enhanced electrical conductivity and magnetic properties. The conductivity of PANI was in the range of  $10^{-10} \text{ Scm}^{-1}$ . Moreover, PANI was a biocompatible and anti-corrosive polymer which has controlled dielectric loss ability. Dielectric materials such as  $\text{TiO}_2$ ,  $\text{SiO}_2$  and  $\text{ZnO}$  were widely used in PCs. At broad GHz range, however, these dielectrics suffer from a lack of permittivity. For this purpose, carbonaceous materials such as graphene, Multi-walled carbon nanotubes (MWCNT) and Reduced Graphene oxide (RGO) have also been used with these polymers.

### **Polypyrrole (PPy) polymer**

Polypyrrole (PPy) was another most promising CP which has poor mechanical stability and process ability due to insolubility and infusibility. To overcome from the above problems, metal nanofillers as inorganic filler can be used with PPy. When the proper combination of suitable nanofillers along with dielectric materials were encapsulated within the PPy PM, then these PCs provide a new standpoint to tune the dielectric and permeability properties of these materials.

### **Poly(3,4-ethylenedioxythiophene) (PEDOT) polymer**

A polythiophene derivative poly (3,4-ethylenedioxythiophene) (PEDOT) possesses a moderate band gap, controllable electrical conductivity, attractive electrochemical activity.

### **Polythiophene (PT) polymer**

Similar to other CPs, polythiophene (PT) was used in anti-corrosion devices, rechargeable batteries and chemical sensors. The conductivity of the PT could be controlled from a conducting to an insulating nature by only changing the polymerization route. Poor solubility of this polymer restrict its use many applications.

### **Insulating polymers nanocomposites (IPNs)**

Though the CPs has many advantages, they suffer from a lack of flexibility and process ability during the large scale production of materials. Hence, IPs likes rubber, resin and other IP composites have been utilized as alternative substrates. With these polymers, synthesis processes were very cheap, easy, time sparing, easy to prepare in large quantities and environmentally stable. To overcome the poor electrical, thermal and mechanical properties of these insulating polymers, metal, alloy and CFs were often mixed into the polymer matrices to enhance the mechanical strength, conductivity and permeability, which improves reflection well as absorption, depending on the filler characteristics. Mostly facile solution mixing, melt mixing and in situ polymerization methods were used for the preparation of these PCs. In the solution mixing method the polymer and fillers were dissolved or dispersed in a common solvent and undergo a stirring and sonication process until the complete mixing / blending of matrix and filler occurs, followed by casting and drying of the as-prepared composites.

### **Polyvinylidene fluoride (PVDF) polymer.**

This polymer was basically piezoelectric in nature, light weight, compact size, good flexibility, and excellent dielectric properties open up the door to wide applications in various fields. PVDF was a semi-crystalline polymer having significant thermal stability and good chemical resistance among polymers. It occurs in five crystalline phases, each with different chain conformations. Pure PVDF has poor EMS properties, but the

addition of NPs within the PVDF matrix improves its conductivity and enhances its response by capitalizing on the nature and properties of the nanoscale filler.

### **Thermosetting polymers**

Versatile thermosetting-resin-based composites offer good adhesion, resistance to corrosion, high strength and stability. These polymers commonly establish a good dispersion and interfacial adhesion between the filler and the polymers. Epoxy resins were one of the important thermosetting resins. In general, polyurethanes (PU) and polyethylene terephthalate (PET) polymers were used to suppress EMI pollution. However, these polymers do not respond in presence of EM waves due to their insulating behavior. Therefore, they were widely used with CPs and carbon materials.

### **Elastomeric polymers**

Elastomers were polymers which exhibit visco-elasticity and were bounded with weak intermolecular forces. These polymers were insulating in nature and have poor physico-mechanical properties. Ethylene-vinyl acetate (EVA), ethylene-propylene-diene monomer (EPDM) and nitrile rubber (NBR) were some examples of these synthetic rubbers. Therefore, these elastomers have been used with CPs or carbon materials to improve their EMI performance.

### **Other polymers**

Other polymers such as polyvinylpyrrolidone (PVP), polyvinyl chloride (PVC), poly(p-phenylenevinylene) (PPV), polypropylene (PP), polyvinyl butyral (PVB), polyvinyl alcohol (PVA), polyethylenimine (PEI) and

polycarbonate, along with blends (PC (polycarbonate)/SAN [poly(styrene-co-acrylonitrile)]) and PCs have also been studied.

### **Carbon nanotubes (CNT)**

Carbon nanotubes (CNTs) were unique one-dimensional (1D) NSs that can be understood hypothetically as a 1D quantum wire. These nanotubes belong to the fullerene family. CNTs were two main types: single walled carbon nanotubes (SWCNTs) and multi-walled carbon nanotubes (MWCNTs). Single walled carbon nanotubes (SWCNTs) were an allotrope of  $sp^2$  hybridized carbon atom, similar to fullerenes. A single sheet of carbon comprises the wall thickness all around the circumference. SWCNTs were a crucial type of CNTs owing to their good electric properties compared to MWCNTs. Because of this, the EM-absorbing properties of MWCNTs and SWCNTs were expected to be altogether different. MWCNTs were most promising 1D material due to their attractive properties. Note that structural disorders, appearing in MWCNTs during their development, were responsible for the unusual electrical and optical properties of MWCNTs. As the result of their high aspect ratio, large surface area and low percolation threshold, MWCNTs were favored as effective fillers rather than SWCNTs in terms of EMS potential. Graphitic carbon, carbon black and carbon coils have also been investigated for EMI applications. Although the large surface area of these fillers improves many properties, the major impedance to using these materials as fillers is the requirement for a high weight % ratio, which deteriorates the mechanical properties in case of these polymers.

### **Methods to improve the EMS**

Hierarchical /porous structure or divalent / trivalent ions substitution to the host materials helps to improve the EMS. There were two factors that mainly affect absorption of EM waves, dielectric loss and magnetic loss.

Permittivity and permeability results from electronic, ionic, dipole, natural or exchange resonance, hysteresis and eddy losses, in which the size, distinct geometrical morphology and crystal structure impacts.

The shielding effectiveness was quantified using four of the following methods.

- Open Field or Free Space Method
- Shielded Room Method
- Shielded Box Method
- Coaxial Transmission Line Method

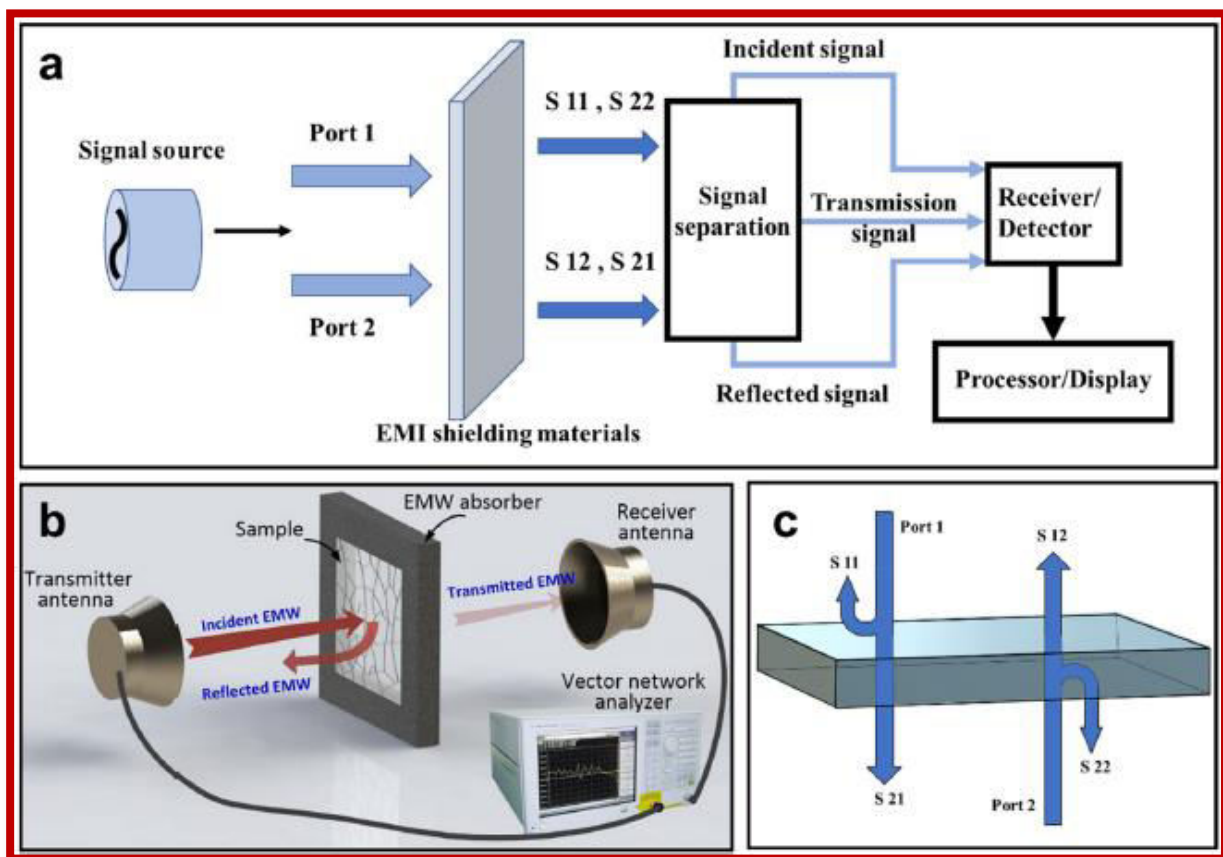


Fig.3 Vector Network Analyzer working principle. [23]

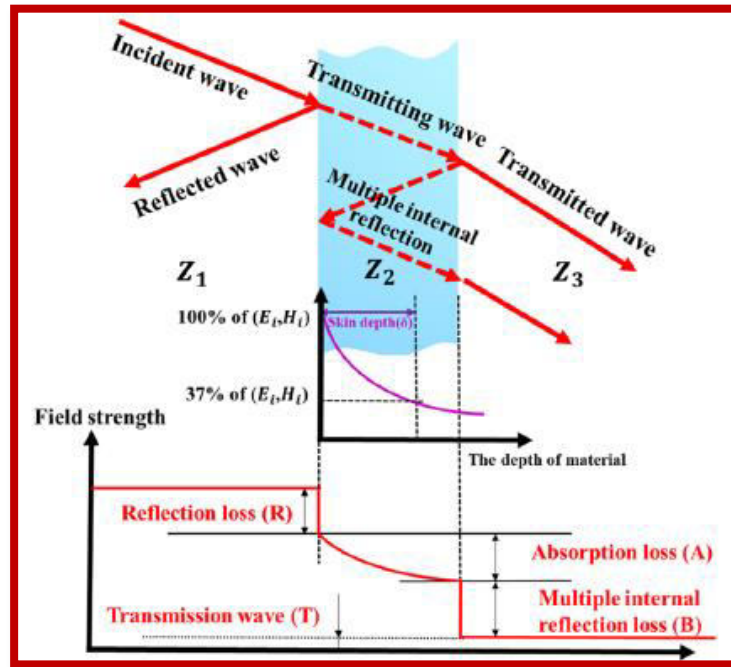


Fig.4. Total mechanism of EMS through the materials [24].

Variety of polymers have been synthesized as the dielectric shells, and coated on the magnetic cores for the improvement of the EM wave absorbing properties [25-28]

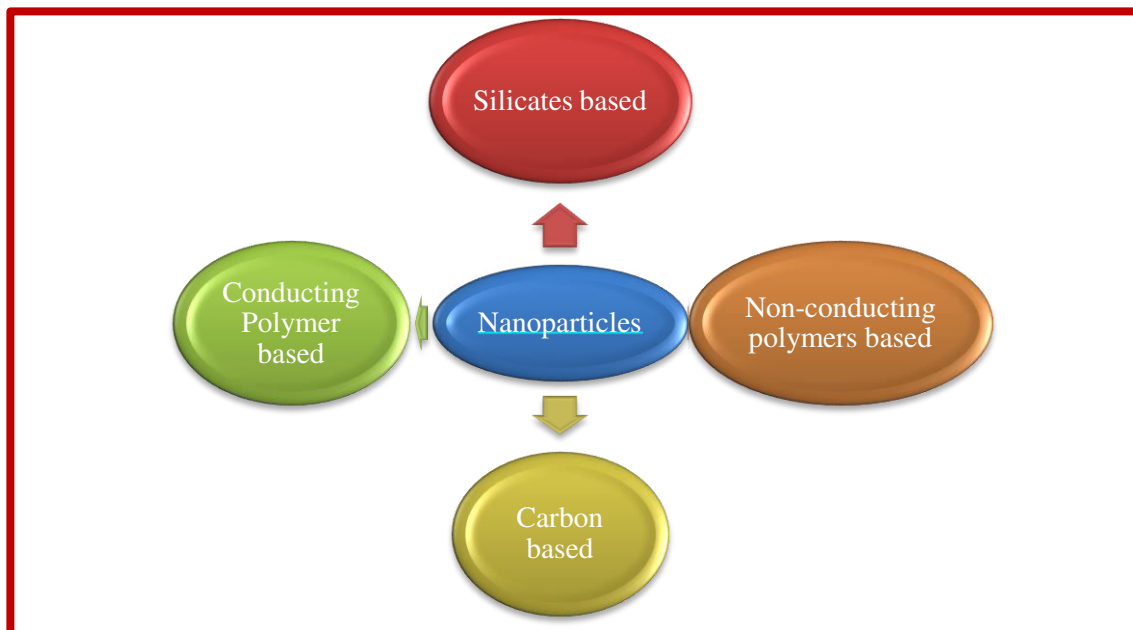


Fig.5 Use of Nanoparticles and their composites for EMS.

Table 1.1.: Various kinds of EMS materials reported and their efficiency towards the total shielding and the dielectric loss.(CP-NCP)

Sl. No	Material	Composition	Crystal Structure	Morphology	Crystallite size and its distribution (nm)	Thickness (mm)	Frequency (GHz)	Reflection coefficient	Absorption Coefficient	Total	Normalized shielding	Skin depth (mm)	tan δ	Reference
1	Conducting polymer based composite by in-situ polymer technique	(Ag/NiFe <sub>2</sub> O <sub>4</sub> /PANI)	Layered Structure	Porous	-	2	8	10	25.17	35.17			-	[29]
							9	9	23	32				
							10	10	7.8	26.5				
							11	8.5	24	32.5				
							12	8.5	26	34.5				
3	PANI coated magnetic nano ferrites such as NiFe <sub>2</sub> O <sub>4</sub> , CoFe <sub>2</sub> O <sub>4</sub> , and ZnF <sub>2</sub> O <sub>4</sub> composites	PANI/CoFe <sub>2</sub> O <sub>4</sub> showed maximum shielding efficiency of 52 dB	Layered	Porous	-	PANI-NiFe <sub>2</sub> O <sub>4</sub> 2 mm	8	--	-	5				
							9	-	-	36				
							10	-	-	35				
							11	-	-	34				
							12	-	-	33				
						PANI-CoFe <sub>2</sub> O <sub>4</sub> 2 mm	8			52				
							9			50				
							10			49				
							11			48				
						PANI-ZnF <sub>2</sub> O <sub>4</sub> 2 mm	12			47				
							8			34				
							9			35				
							10			38				

							11			40				
							12			45				
5	CNT/poly mide foams (CNT/PI) Maximum with CNT	CNT,PI,C P11,CP12, CP21	Layered	Porous		2mm	8			38				[30]
							9			39				
							10			40				
							11			41				
							12			42.5				
6	MXene- based CPC foams MXene@P ANI/mPP by batch foaming method	MXene 0.0449 - optimized	-	Closed - Cell structure	-	12mm	8			39.8				[31]
7	Shape- memory carbon foam composites <i>trans</i> -1,4- polyisopren e (TPI)- MXene layer solution mixing and vacuum drying	Hexadecyl trimethyl ammonium Bromide (CTAB)/M Xene- 0,5,10,20w t%	Semi crystallin e	Cellular oriented multi microstrur e		10mm	8			45				[32]
							9			46				
							10			47				

	method.						11			47.7				
							12			44				
10	MXene/ polydimeth ylsiloxane by spin coating process	Optimized 11 layers of Mxene/PD MS/ boron nitride					8			31				[33]
							9			32				
							10			33				
							11			35.2				
							12			32.5				
8	poly (vinyl alcohol)/tra nsition metal carbide (PVA/MXe ne) multilayer d films by multilayer d casting method	MXene- 19.5wt% was optimized		Multilayer red structure		12mm	8			44				[34]
							9			42				
							10			45				
							11			44				
							12			45				

9	Polyurethane	MWCNTS - 48.1wt% Optimized		3 dimensional network		2mm	8			29				[35]
							9			28				
							10			27.5				
							11			27				
							12			26				
10	Polymer nanofibers	Copper-wrapped	Cellular microstructure			50 $\mu$ m	8			75				[36]
							9			76				
							10			76.8				
							11			70				
							12			69				
11	Polyimide prepared by ultrasonication	5% short carbon fiber and 4% carbon black - Dopants		Bridge like structure		0.35	8	9	14	23				[37]
							9	7.5	15	22.5				
							10	8	15	23				
							11	8.9	14	23.9				
							12	7.5	16	23.5				
12	PDMS	Graphene -		Lamellar		5mm	8			59			0.0	[38]

	bidirectional freezing technique	0.42wt%		structure			9			60			
							10			59			
							11			62			
							12			65			
13	Ti <sub>3</sub> C <sub>2</sub> T <sub>x</sub> -MXene dyes Coated Fabrics by Acid aqueous LiCl solution method	Cotton-54wt% Linen-48wt% coated with cotton-0,54,42,36,28,21,14,0 wt% and coated with linen-0,10,16,22,29,34and 48wt%					8cotton			78			[39]
							9			80			
							10			81			
							11			80			
							12			75			
							8Linen			80			
							9			78			
							10			79			
							11			81			
							12			79			
14	CCA@rGO /PDMS( cellulose carbon aerogel by freeze drying and vacuum impregnation method with 3.05wt%CCA	Optimized composition <a href="#">CCA@rGO/PDMS</a> CCA@rGO - <a href="#">PCCA@rGO-3.05</a>		Skin core structure	10mm		8			52			[40]
							9			53			
							10			54			
							11			55			
							12	44	7	51			

15	MXene Ti3C2Tx composite film by incorporating of poly(3,4-ethylenedioxythiophene)/poly(styrenesulfonate) (PEDOT/PSS) by vacuum assisted filtration	PEDOT/PSS-30wt% Mxene- 90 wt%			Accordion like stack	6.6µm	8			44.5				[41]
							9			44.00				
							10			43.5				
							11			43				
							12			42.5				
16	Polyurethane@polydopamine sponges by dopamine self-polymerization. (ii) <i>in-situ</i> electroless plating method	Silver NPs	Face centre cubic		15nm		8	11.5	71.5	83				[42]
							9	11	71	82				
							10	11.25	69.75	81				
							11	11.5	72.5	84				
							12	11	70	81				
17	PVA	GO/NiO	Semi						12				[43]	

	by solution casting technique	/Chitoson/ PVA 3.0/30 /17/50 wt%	crystalline				12							
18	Polystyrene and polyaniline - solution casting method with PANI 40wt%	PANI-20,40wt%	Amorphous in nature		interconnected network structure	250 micron	8	0	48	48				[44]
							9	0.5	46.5	47				
							10	0.8	47	48				
							11	1	37	38				
							12	1.2	32.3	33.5				
19	PVC/	Thermally Reduced Graphene Oxide, Polyaniline ,Polyvinyl chloride) nanocomposites with 0wt%	-	homogenous dense interconnected network	26 nm	0.25-0.1	8	75	26	101				[45]
							9	73	25	98				
							10	65	35	100				
							11	70	35	105				
							12	70	32.5	102.5				
20	(rGO@Fe3O4, [RGF]))+P	1.CNT/RGF/PC(CFP) with CNT	Crystalline	Macroscopic network	237.9 μm diameter	2 mm	8	5	38	43				[46]
							9	5	38	43				
							10	5	38.5	43.5				

	C+CNT wrapped outside (polycarbonate – PC) by solution mixing method	– 1,2,3 and 4 wt% 2.CNT/PC (CP) CNT-1,2,3,4wt %	structure	high EMI SE of 43.5 dB with a SEA/SET ratio of ~90%.	size		11 12	5 5.5	39 39.5	44 45				
21	MS-g-PANI/paraffin wax composites (vinyl modified sepiolite (MS)) by mixing method	Grafting PANI-46,294,644wt%	Crystalline structure		splitted fibrous structure  X-band frequency range (24.2 dB) opens new possibilities of developing conducting nanohybrids	5mm	8 9 10 11 12	7 7.5 7.5 8 8	15 15 15.3 15.3 15.5	22 22.5 22.8 23.3 24				[47]
	Nickel-plated porous calcium silicate by Hydrother	Ni/PCS 10/1 was optimized	Wollastonite - Monoclinic	cauliflower-shaped - core-shell structure	4-7	0.9	8	9	41	50		0.2	-	[48]

	mal method													
	Carbon-Al <sub>2</sub> O <sub>3</sub> -SiO <sub>2</sub> (Cenosphere) Composite Foams prepared by Polyurethane template	CCF-cenosphere 30wt% was optimized	Monoclinic	spherical in shape with small pores on the surface. Particle size distribution ~ 65 µm.	0.3424nm	0.45	8	6	42	48		0.5	0.7	[49]
	Polystyrene-Cu Nanowires prepared by solution blending Cu NWS2.1 Vol%	Cu NWS-2.1Vol% optimized		-	-	0.21	8	-	-	35		0.1	-	[50]
	Reduced graphene oxide (rGO) and Fe <sub>3</sub> O <sub>4</sub> @SiO <sub>2</sub>	rGO:Fe <sub>3</sub> O <sub>4</sub> @SiO <sub>2</sub> -4:1 was optimized	Monoclinic	semicircular shape	250	2	8	7	19	26		0.9	-	[51]

prepared by solvothermal method-4:1 wt %														
Epoxy/Polysulfone/Multi-walled Carbon Nanotubes (EP/PES/MWCNT) composites were prepared by ultrasonic treatment and dichloromethane-assisted dispersion	MWCNT-4.8wt%, PES-23,	-	Spherical shape-10µm		2.2	8	5	23	28		0.7	-	[52]	
PANI/SnO composites	PANI/SnO-1, PANI/SnO-20/3 wt% was optimized	-	-	-	2	8			23		-	-	[53]	

MWCNT/ PS 7 wt%	MWCNT/ PS 7wt% was optimized	D				1.2	8-12			19				[54]
Go@Fe <sub>3</sub> O <sub>4</sub> @ cusilicate by Brunauer– Emmett–T eller method	1:1 was optimized	monoclin ic	3D hierarchi cal structure s	~31 nm.		1	8	5	36	41				[55]
EVA/GP/ MP/OMM T/SCF composite by twin- screw extruder	EVA/GP/ MP/OM MT/SCF composite 35/23/17/ 5/20 Was optimized	-	continuo us electro- conducti ve network	-		~ 2.6	8	8	28	36				[56]
PAT compositi on MXene– PAT– PANI– PpAP composite (MXPAT PA) by spray coating	MXene– PAT– PANI– PpAP		Farm structure			0.062	8	9.18	35	44.18				[57]



	Process													
--	---------	--	--	--	--	--	--	--	--	--	--	--	--	--

Besides the intrinsic polarizations of monomers and defects, amorphous polymer shells coated on the crystalline magnetic cores bring dipole-dipole interactions and interfacial polarizations by the radicals and dangling bonds, which also greatly impact the relative permittivity and dielectric attenuation [58]. Appropriate adjustment of dielectric properties was an effective way to improve the poor input impedance in the core/shell absorbers.

---

### **Cellulose carbon aerogel@reduced graphene oxide aerogels**

Song et al prepared the cellulose carbon aerogel@reduced graphene oxide aerogels (CCA@rGO) by vacuum impregnation, freeze-drying followed by thermal annealing and finally the CCA@rGO/polydimethylsiloxane (PDMS). EMS composites were prepared by backfilling with PDMS (Fig.6). PDMS/n-hexane temperature was raised to 65 °C for 4 h. Prepared samples were carbonized at 1500 °C under nitrogen atmosphere for 2h to obtain cellulose carbon aerogel. Fig.7 shows the schematic diagram of the prepared samples. Type-I cellulose was confirmed by XRD with a graphitic carbon on (002) and (100) planes which were attributed to high temperature carbonization of samples. Raman, FTIR and XPS studies were performed to show the nano-regime of prepared samples. Morphology of these samples showed the fibers/ rod like structure with a good network and showed single fibers of CCA with approximate diameter of 6  $\mu\text{m}$ . Loading of PCCA was 2.80 wt% changes the  $\sigma$  of the PCCA/PDMS composites to  $0.094 \text{ Scm}^{-1}$ . The synergy of the two conductive networks improved the internal conductive network of the composites and the consequent  $\sigma$  also increased. Authors reported that wrapped CCA with 3D double-layer conductive network with PDMS were prepared with 3.05 wt% showed the best shielding of 51 dB (Fig. 8). Its thermal conductivity was  $0.65 \text{ W mK}^{-1}$  shows that these materials with lightweight were more suitable for the flexible EMS and portable electronic devices.

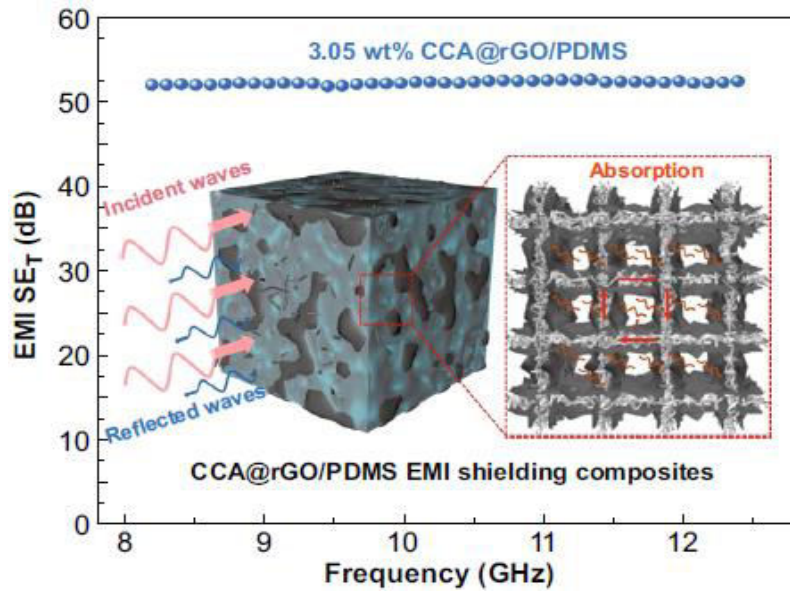


Fig 6: Composition of CCA@rGO/PDMS EMS composites.

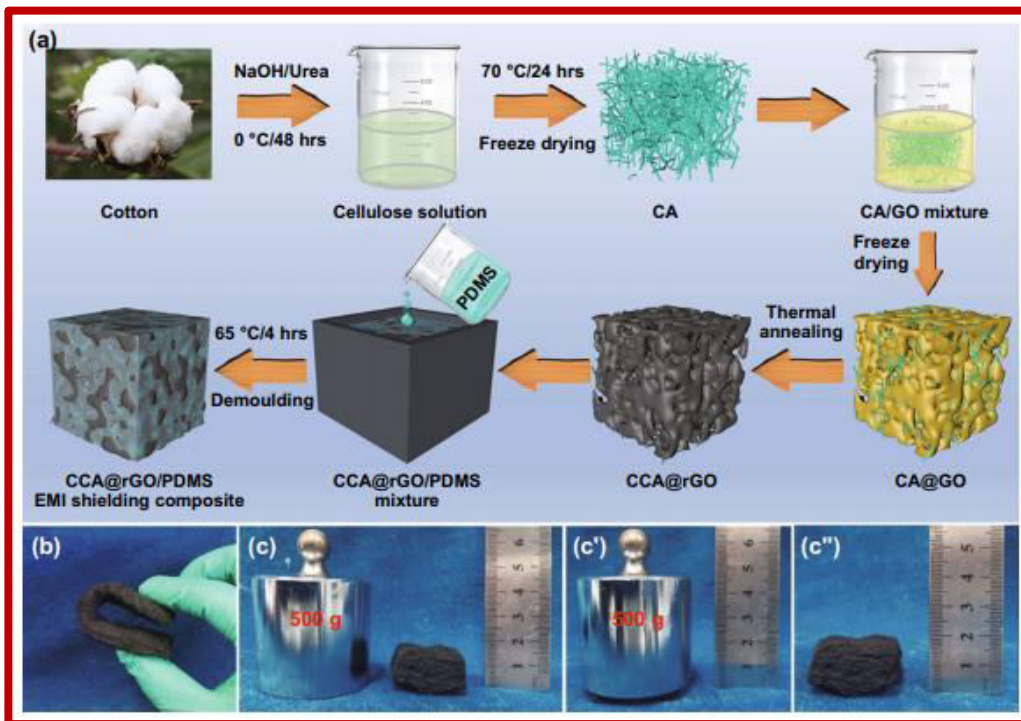


Fig.7. Fabrication procedure for CCA@rGO/PDMS (a), illustration of the flexibility (b) and resilience (c-c'') of CCA@rGO aerogel. [59]

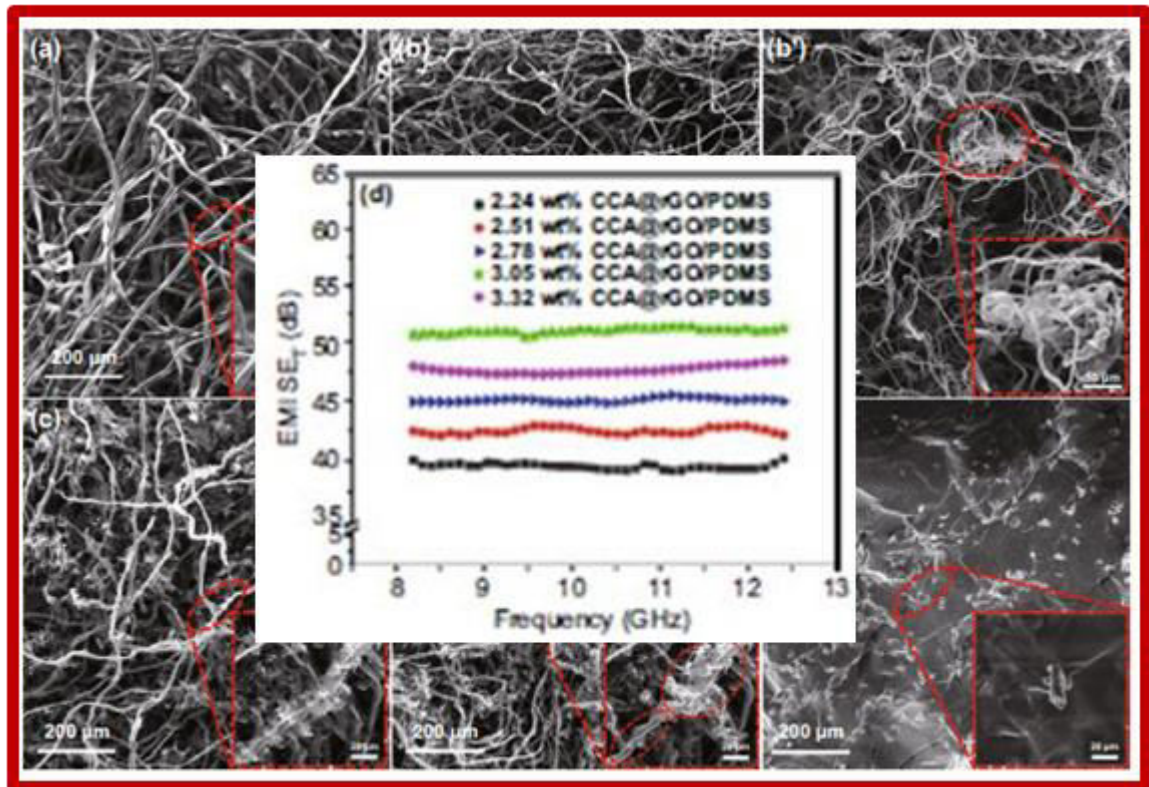


Fig.8 SEM images of CA (a), CCA (b-b'), CCA@rGO (c-c') and the CCA@rGO/PDMS composites (d) EMS of the samples showed highest for the 3.05 wt% of CCA@rGO/PDMS.

### Mxane composite

Xichen et al., prepared compressible CPC of PDMS/MPFB foams by assembling MPFBs into 3D accumulation with MXene networks followed by the encapsulation of PDMS (schematic diagram-Fig. 9A). SEM images of PP foam cells and PDMS/MPFB composite foams showed the PDMS skeleton and interface between MXene@PANI/mPP foam beads were seen. They were orderly arranged in a mold and then were immersed in PDMS solution which was cured for the better adhesive. In the preparation, hydrophilicity was altered by using  $\text{KMnO}_4$  and HCl.

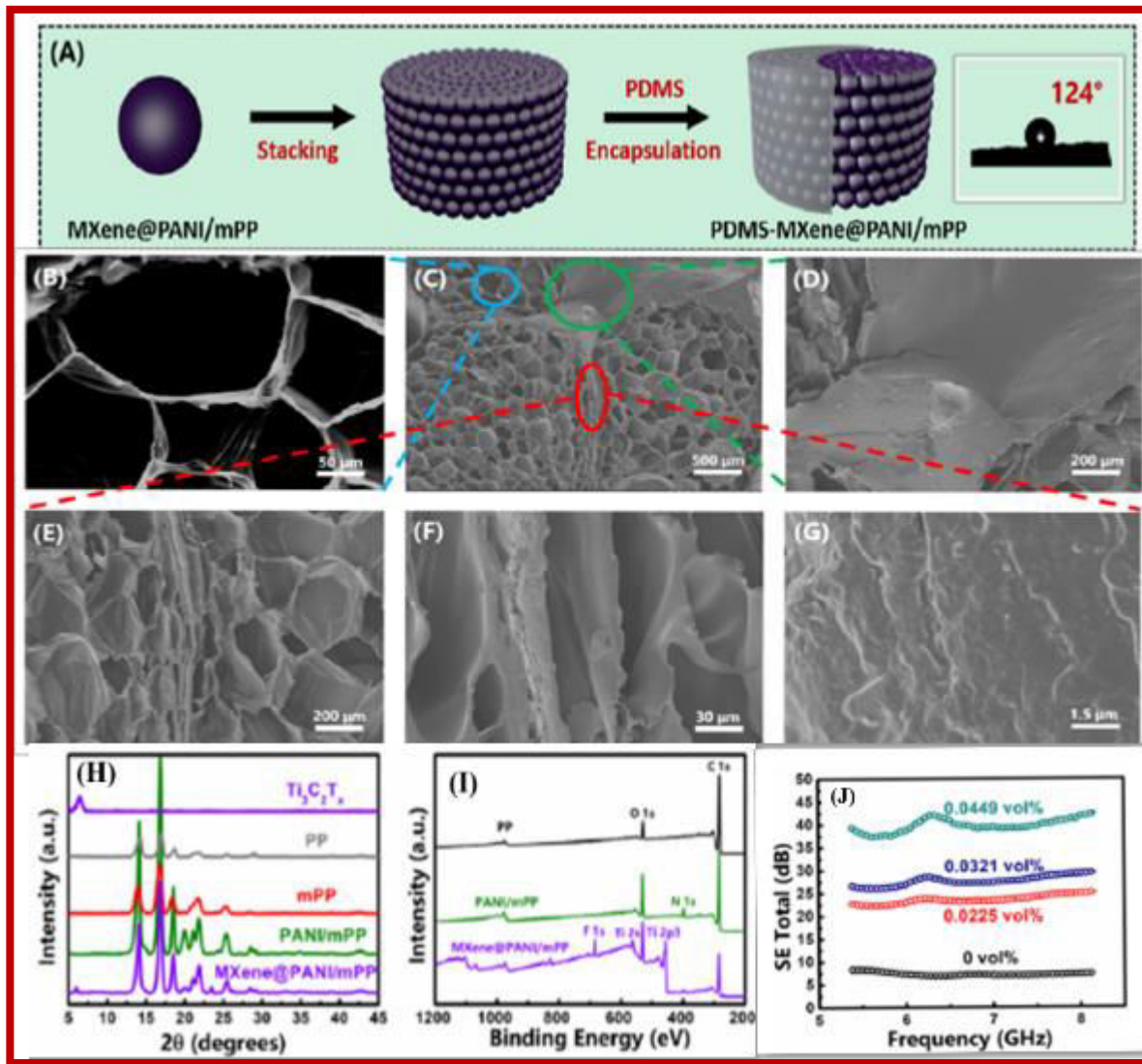


Fig. 9. MXene@PANI/mPP composite foams (A) Schematic illustration of the encapsulation process of PDMS/MPPB composite foams. SEM images of (B) PP foam cells, (C) PDMS/MPPB composite foam, (D) PDMS skeleton and (E, F, G) interface between MXene@PANI/mPP foam beads, (H) PXRD profiles of all the prepared samples. (I) XPS of PP, Pani/mPP and MXene composite (J) SE Total for different volume percentage. [60]

Measured contact angle of the samples surface was done to tune their surface from hydrophilic to hydrophobic nature. This can be seen clearly in the SEM images as in Figs. 9B to 9G shows the skeleton of PDMS and the interface of the polymer with the foam beads. Dense layer of MXanes and strong adhesion between PANI-

MXene were observed. They showed excellent EMS performance of ~23.5-39.8 dB with only ~0.0225-0.0449 vol% MXene. Ultimate EMI of 39.8 dB was obtained for 0.0449 vol% MXene, 0.02 vol% of PANI and  $SE_R$  of 0.31 (Fig. 9J). Highest  $SE_T$  was observed for 12 mm thickness of the samples and was stable in the frequency range of 5.5 to 8 GHz. XRD peak of  $Ti_3C_2T_x$  MXene at  $\sim 6^\circ$  appeared reveals the successful decoration of MXene nanosheets via a dip-coating approach (Fig. 9H). Presence of N1s peak in the XPS curve of PANI/mPP foam was observed and it was disappeared for the MXene composite. Both hydrogen and covalent bonds presence enhanced the structural stability of PANI/mPP foam beads. With this ultra-low R coefficient of ~0.05 was obtained with effective EMS of ~23 dB at total MXene content of ~0.0225 vol%, which was the lowest R value for effective EMS.

#### **MXene/PDMS/BN composite with enhanced thermal conductivity for EMS application**

Liu et al., altered multilayer films of MXene/PDMS/boron nitride (BN) with different composition were prepared by layer-by-layer spin coating process to simultaneously achieve EMS as showed in Fig.10 [60]. Heat dissipation and electrical insulation with special multilayer structure allows EM waves to reflect and absorb multiple times between the composite layers. The conductive networks (CNs) were in-plane constructed and the BN/PDMS layers insulate the conductive path through vertical plane and provide effective heat dissipation for multilayer films. The EMS of the multilayer film with 11-layers structure can reach 35.2 dB at 10.9 GHz. This showed new light on the development of multifunctional composites, which can be envisioned as an advanced electronic packaging material also.

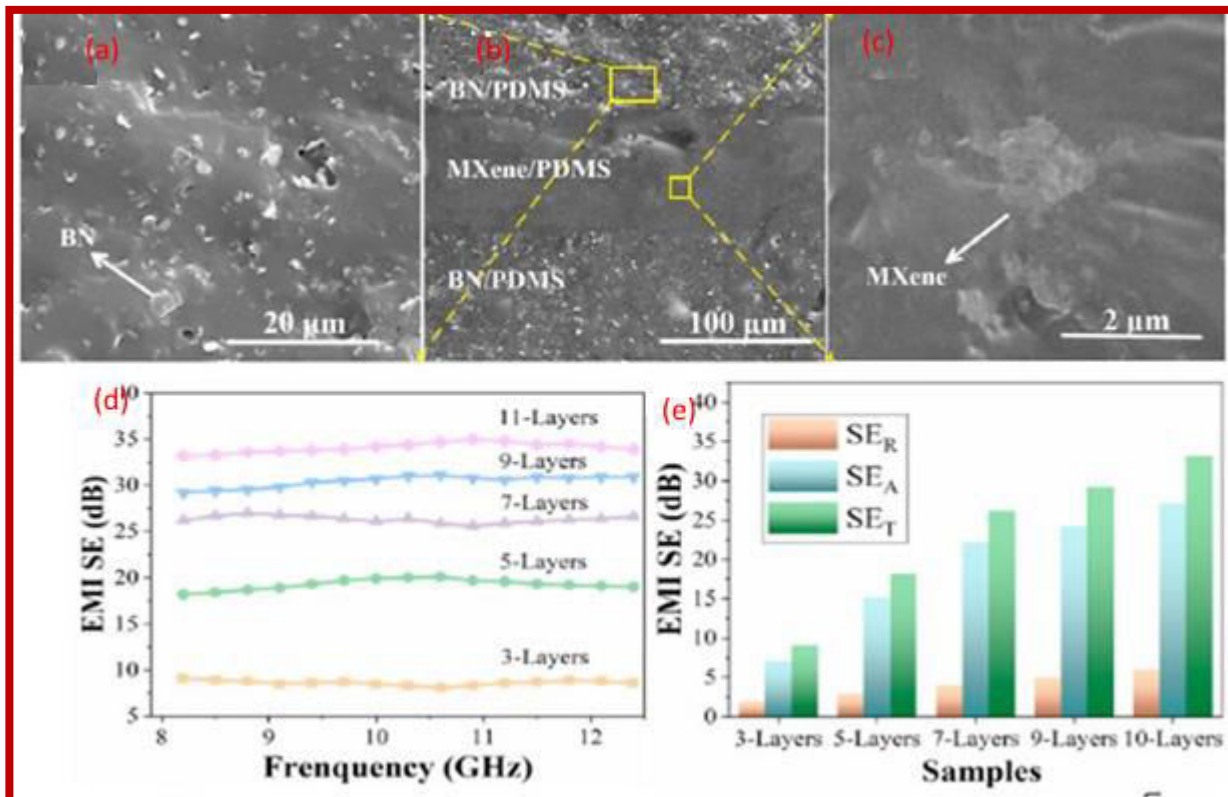


**Fig. 10.** (a) Scheme of the preparation process of the multilayer films; SEM images of fractured surfaces of (b) BN/PDMS layer; (c) 3-Layers; (d) EMI SE of multilayer films with different layers in the frequency range of 8.2–12.4 (e) MXene/PDMS layer.

Wan et al., reported a flexible MXene/PC film by cooperating of PEDOT:PSS and treatment with concentrated H<sub>2</sub>SO<sub>4</sub> to remove the insulating PSS which improves EMS. With 30 wt% PEDOT:PSS into Ti<sub>3</sub>C<sub>2</sub>T<sub>x</sub> film and by acid post-treatment, the EMS of composite film with thickness of ~6.6 μm showed SE<sub>T</sub> up to 40.5 dB and the increment in tensile strength was 155% high when compared to that of Ti<sub>3</sub>C<sub>2</sub>T<sub>x</sub> film. The combination of mechanical and EMS portfolio outperforms the counterpart of other PCs filled with MXene-H up to 70wt%. The microstructures of the MXene film and MXene/PC films with different loading before and after post-treatment were revealed by SEM as shown in Fig. 11 (a). MXene sheets were exposed and more easily to be observed in the composites (Fig. 11b and c) due to the removal of PSS. The overall performance was much better than that of reported MXene/PC, such as MXene/cellulose fiber and

MXene/wax. This work paves a new way to fabricate light-weight, flexible, mechanically strong and high-performance EMS materials.

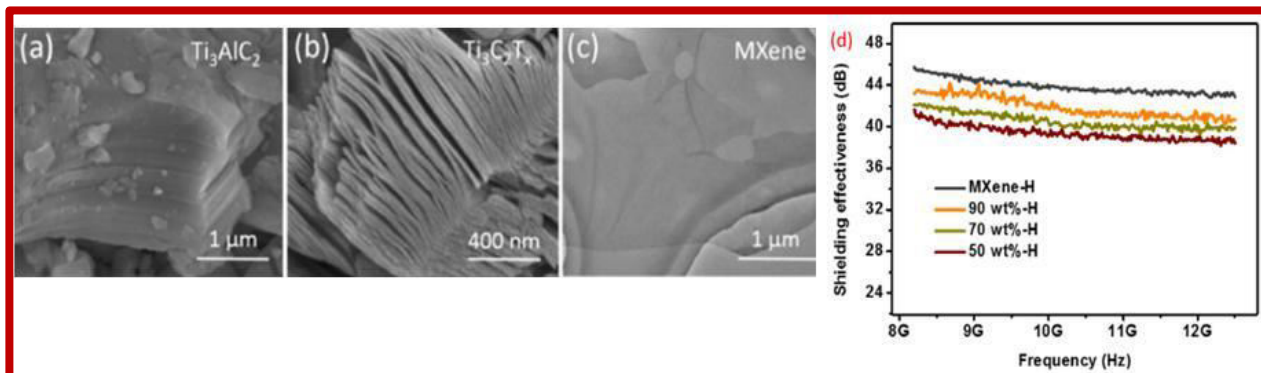
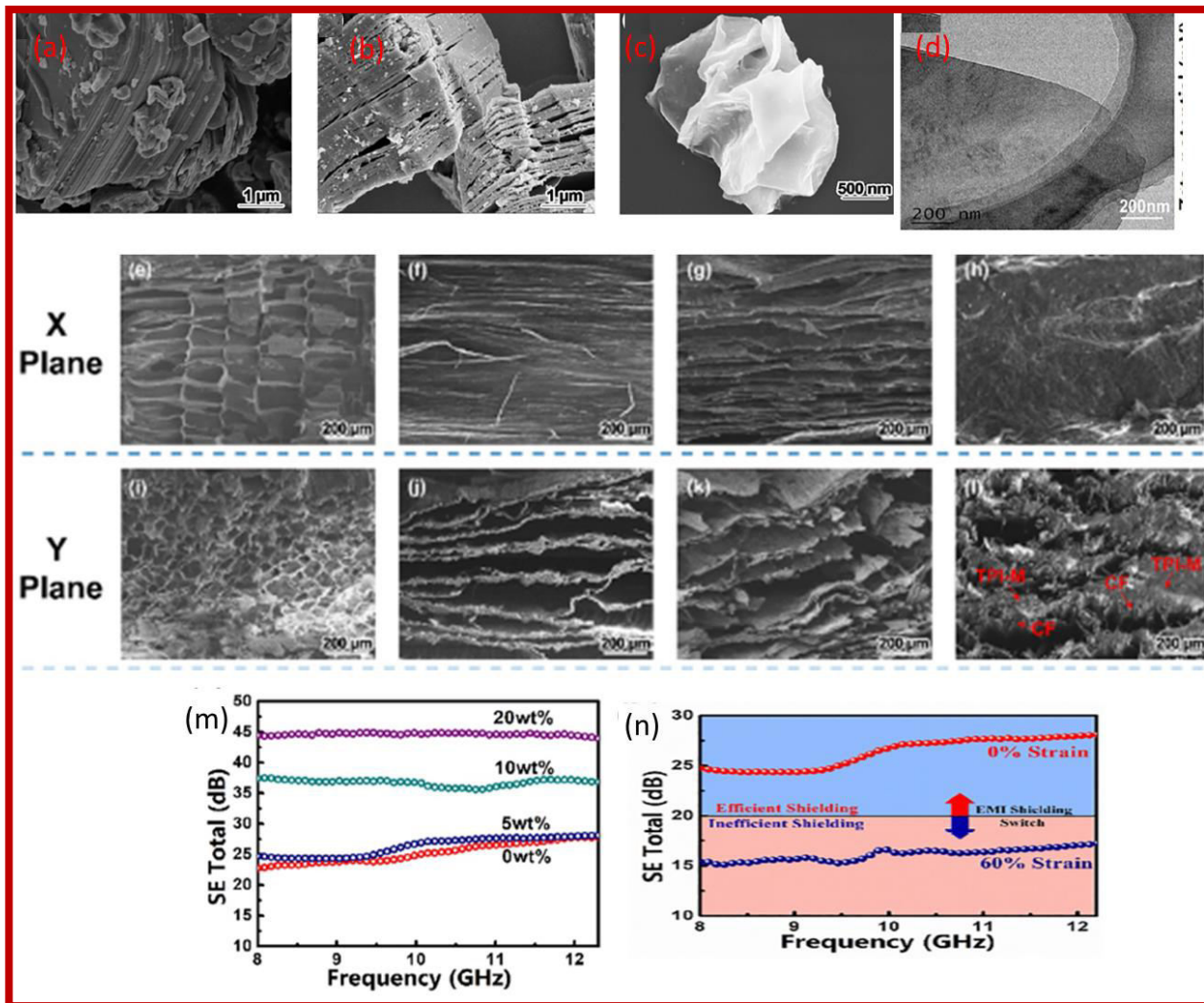


Fig 11(a) SEM image of  $Ti_3AlC_2$  before etching; (b) microstructure of  $Ti_3C_2T_x$  after etching, showing the loose layered structure; (c) TEM image (d) EMI SE.

### Composites of carbon foam coated with TPI-MXene

Xichen Jia et al., adopted pyrolysis of chemically treated Balsa wood, and *trans*-1,4-polyisoprene (TPI) as a polymer matrix (PM) compressible carbon foams (CF) with multilayer microstructure were fabricated (Fig. 12). In the preparation, hydrophilicity was altered by using  $KMnO_4$  and  $HCl$  which was confirmed by the contact angle technique. Wave-guide method to measure EMS recorded the  $SE_T$  of neat TPI/CF (without MXene) was as high as  $\sim 25.3$  dB, which indicate that  $\sim 99\%$  of incident microwave was shielded. With the TPI/MXene coating, the  $SE_T$  of TPI-M/CF with  $\sim 5$ ,  $\sim 10$ , and  $\sim 20$  wt% CTAB-MXene was enhanced to  $\sim 26.3$ ,  $\sim 36.7$  and  $\sim 44.7$  dB, verifying the shielding enhancement because of more and more efficient conductive MXene networks. Composition variation of TPI / CF and MXene helps to obtain the desired shielding effects.



**Fig. 12.** (a–c) SEM images of (a) Ti<sub>3</sub>AlC<sub>2</sub>, (b) clay-like Ti<sub>3</sub>C<sub>2</sub>T<sub>x</sub> and (c) few-layer curled Ti<sub>3</sub>C<sub>2</sub>T<sub>x</sub> sheet. (d) TEM image of flat Ti<sub>3</sub>C<sub>2</sub>T<sub>x</sub> sheet. (e–l) XRD patterns of Ti<sub>3</sub>AlC<sub>2</sub>, Ti<sub>3</sub>C<sub>2</sub>T<sub>x</sub> and CTAB-Ti<sub>3</sub>C<sub>2</sub>T<sub>x</sub> hybrid, (m). SE Total of TPI-M/CF composite and (n) SE Total of TPI-M/CF composite (~5 wt% CTAB-MXene) with different compressive strains, exhibiting function-switchable EMI-shielding behavior.

Reaction of HF with Al layers of Ti<sub>3</sub>AlC<sub>2</sub> produced large amount of H<sub>2</sub> helped in creating the interlayer space of clay-like Ti<sub>3</sub>C<sub>2</sub>T<sub>x</sub> which after ultrasonication exfoliation changes the structure to flat lamellar as showed in Fig. 12(e-l). With increased MXene loading nearly 20wt%, SEM images show a channel-like and grid-like

microstructure in the X- and Y-planes respectively. These prepared composites showed the  $SE_T$  of 44.7 dB at 10 mm thick and in the frequency range of 8 to 12 GHz, SET value was almost constant.

Zhao et al., reported that cellular structure in CPCs as an effective way to revolutionize the EMS properties and conductive PVDF / MWCNT CFs fabricated through a simple and effective batch foaming process [61] . Highly conductive and hydrophobic PVDF/MWCNT CFs were obtained by controlling the MWCNT content and impregnation temperature. For PVDF/5 wt% MWCNT and PVDF/8 wt% MWCNT NCFs, EMS properties gradually increased with an increased degree of foaming in the range of 27–40 wt%. The highest EMS of 132.6 dB was obtained for the second CF with a sample thickness of 4.0 mm. Fig 13(a) shows the schematic mechanism of absorption resulting from multiple reflections, scattering and strong conduction band polarization loss were the main contributing factors. SEM images (Fig13(b-h)) showed the possibility of incorporation of a cellular structure into the PVDF/WMCNT composites effectively to tune their EMS properties.

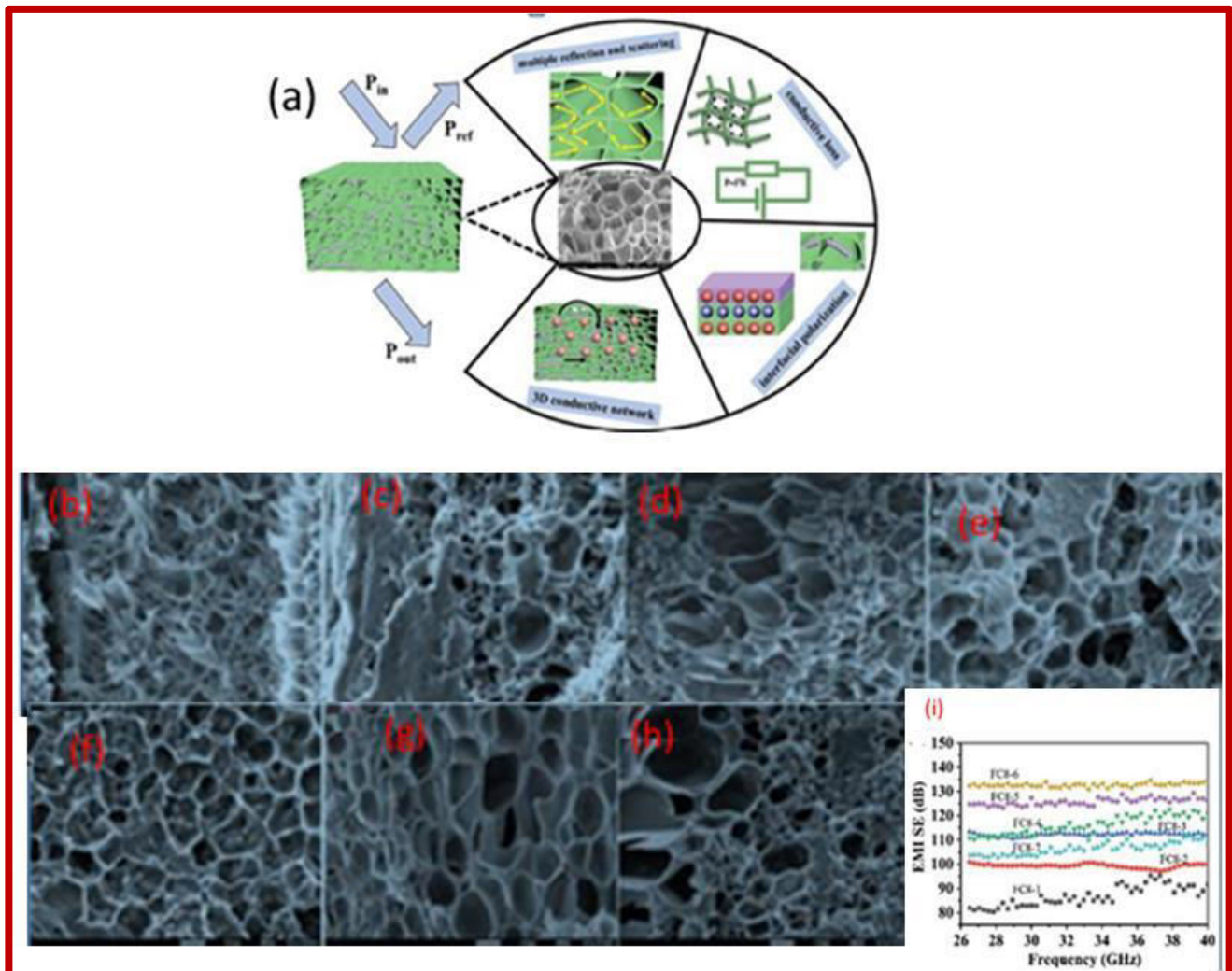
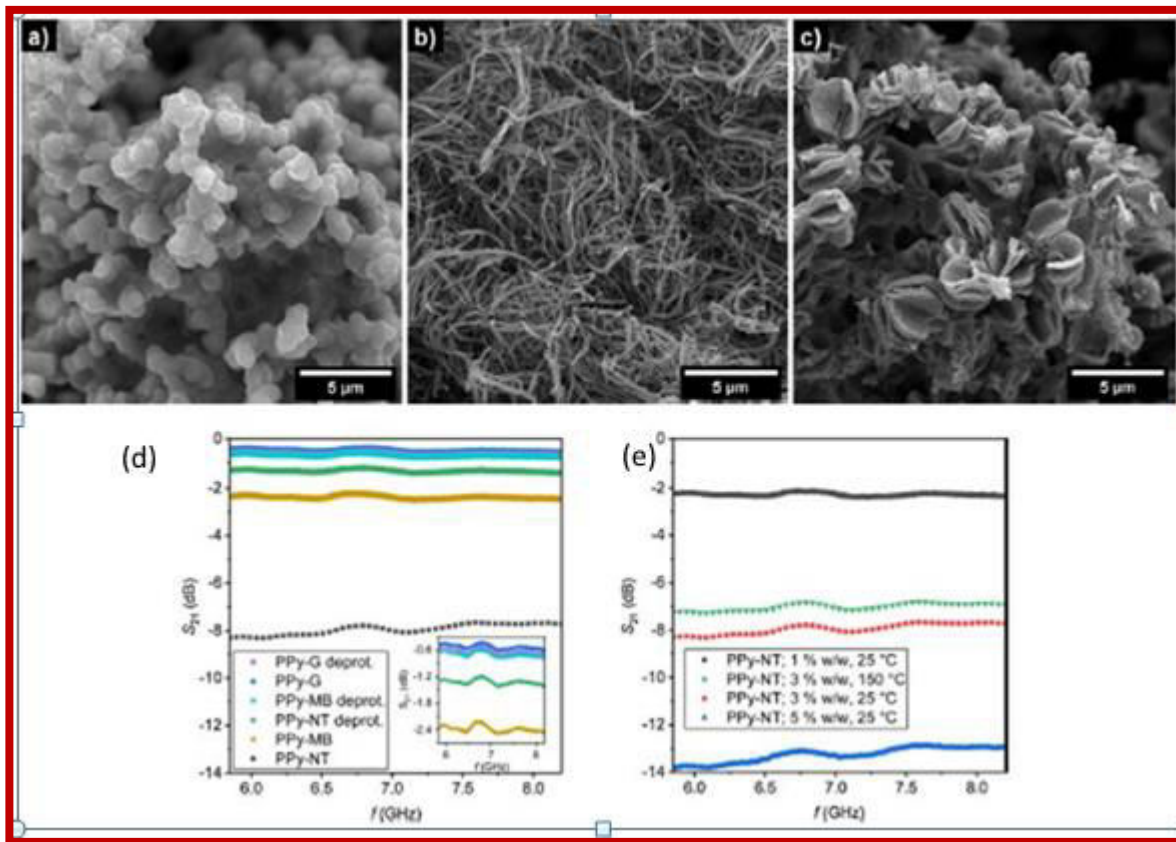


Fig :13(a) Schematic illustration of EM wave transmission across the PVDF/MWCNT nanocomposite foams and its related shielding mechanism.,(b-h) SEM images of the cryo-fractured FC8 nanocomposite foams: (b) FC8-1, (c) FC8-2, (d) FC8-3, (e) FC8-4, (f) FC8-5, (g) FC8-6 and (h) FC8-7 samples.(i) EMI blocking abilities of various PVDF/MWCNT nanocomposites of FC8 foams

### EMS of polypyrrole nanostructures

Robert et al., reported the PPy prepared with various morphologies such as globules, nanotubes and microbarrels [63]. Here the powdered samples in both protonated and deprotonated form with different concentrations (1, 3 and 5 % w/w) in a composite system with a transparent silicone matrix cured at

temperatures 25 and 150 °C. PPy have an ability to reflect or absorb EM radiation in the C-band region covering the range from 5.85 to 8.2 GHz. The PPy NT with the DC conductivity of  $60.8 \text{ S.cm}^{-1}$  exhibited SE  $S_{21} = -13.27 \text{ dB}$  at 5% w/w concentration in the composite, which corresponds to transparency of 21.7 % only. The morphology of all the prepared PPy powders was presented in the Fig. 14(a-c). Both PPy-G and PPy-NT have uniform particles, each with their respective size lying in a relatively narrow range; PPy-G particles were around 1  $\mu\text{m}$  in diameter and PPy-NT were around 60–80 nm in diameter and several  $\mu\text{m}$  long. Uniformity of PPy-MB depicted in the Fig. 12c did not reach such level as in the case of PPy-G and PPy-NT. However, the vast majority of PPy-MB has micro barrels with around 3  $\mu\text{m}$  in diameter composed of plates 300 nm thick, some of them with small defects and minor part comprises globular particles of PPy due to the polymerization of pyrrole outside the template. The PPy-NT and PPy-MB exhibit higher aspect ratio compared to PPy-G. The PPy-NT and PPy-MB also inevitably contain small content of azo-dye remnants (up to 1 % w/w), some of them as dopants, some of them as a composite component, which was present in small cavities of particles.



**Fig 14.** The morphology of prepared PPy powders: a) globular (PPy-G), b) nanotubular (PPy-NT), c) polypyrrole microbarrels (PPy-MB). (d). The EMS properties of PPy structures and their deprotonated counterparts (3 % w/w, 25 °C); detailed overview of PPy samples with low shielding efficiency (SE) in the inset and e) PPy-NT at various filler loadings and temperatures of sample preparation [62]

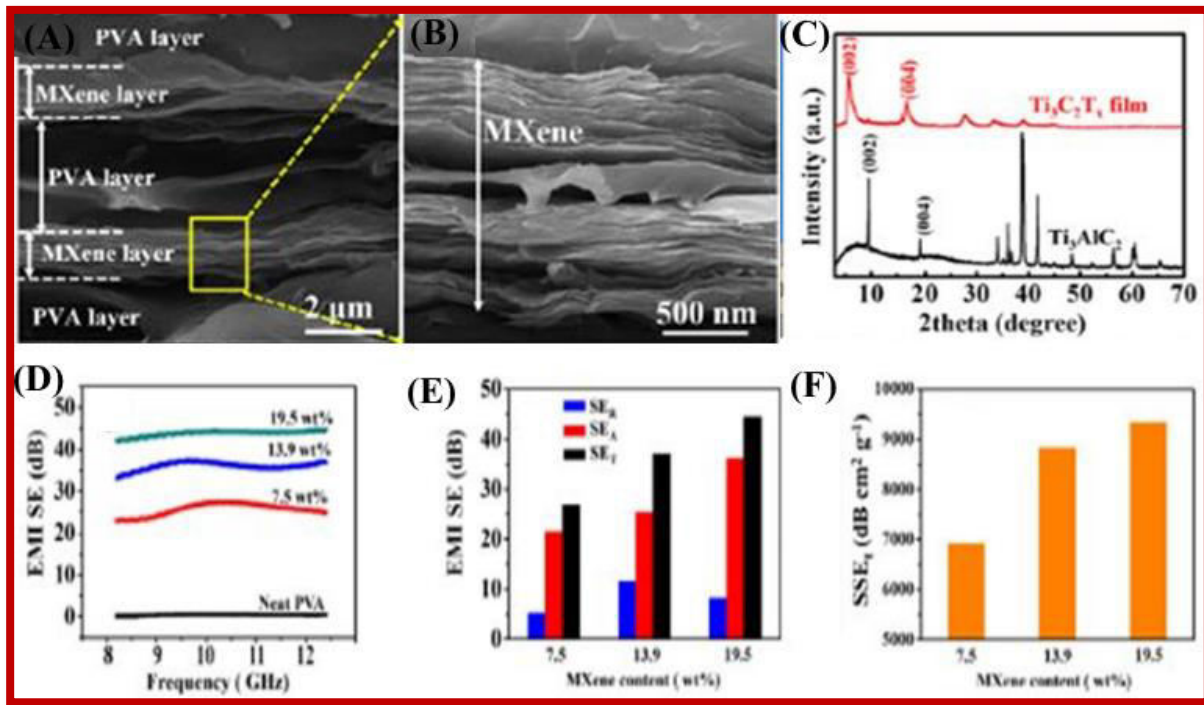


Fig. 15. A) & B) SEM images of the prepared samples with different magnifications. C) XRD patterns of  $Ti_3AlC_2$  and  $Ti_3C_2T_x$ -MXene film, respectively D) EMI SE of neat PVA and different PVA/MXene multilayered films in the X-band E) comparison of  $SE_T$ ,  $SE_A$ , and  $SE_R$  of different PVA/MXene multilayered films at 10 GHz; (F) Specific SE accounting for the thickness ( $SSE_T$ ) of different PVA/MXene multilayered films. [64].

## Conclusions

It was found the magnitude of electrical conductivity together with the aspect ratio of polymer morphology determines the SE whereas the type of morphology was responsible for absorption or reflection mechanism of EMS. Hence, the appropriate adjustment of both the electrical conductivity and the morphology should be used in the future lightweight and flexible EMI shields with tunable SE and mechanism of shielding.

Graphene, CNTs, Mxanes were found as the potential lightweight materials along with the suitable polymers are the most expected packing and shielding materials. Still there is a lot of research need to be done in this field where the materials of very thin will have great flexibility and also excellent EMS for the wide range of frequency is the motto of future research.

## References

- [1] X. Jian, B. Wu, Y. Wei, S. X. Dou, X. Wang, W. He, N. Mahmood, *ACS Appl. Mater. Interfaces*, 2016, 8, 6101–6109.
- [2] S. R. Dhakate, K. M. Subhedar and B. P. Singh, *RSC Adv.*, 2015, 5, 43036–43057.
- [3] V Shukla, *Nanoscale Adv.*, 1 (2019) 1640-1671.
- [4] R. Che, C. Zhi, C. Liang and X. Zhou, *Appl. Phys. Lett.*, 2006,88, 033105.
- [5] G Wang, J Zhao, C Ge, G Zhao C B Park, *Journal of Materials Chemistry C* 9 (2021) 1245-1258.
- [6] S. Geetha, K K Satheesh Kumar, Chepuri R K Rao, M Vijayan, D C Trivedi, *J. Appl. Polym. Sci.*, 112(2009) 2073-2086.
- [7] Panwar V, Kang B, Park J O, Park S and Mehra R M, *Eur. Polym. J.* 45 (2009) 1777–1784.
- [8] N. Maruthi, Muhammad Faisal, Narasimha Raghavendra, *Synthetic Metals*, Volume 272(2021) 116664.
- [9] Yao, Y., Jin, S., Zou, H. *J Mater Sci* 56 (2021) 6549–6580.
- [10] Y. Jia, T.D. Ajayi, B.H. Wahls, K.R. Ramakrishnan, S. Ekkad et al., *ACS Appl. Mater. Interfaces* 12 (2020) 58005–58017.
- [11] N. Yousef, X. Sun, X. Lin, X. Shen, J. Jia, *Adv. Mater.* 26(31)(2014), 5480–5487.
- [12] J. Ju, T. Kuang, X. Ke, M. Zeng, Z. Chen et al., *Compos. Sci. Technol.* 193(2020)108116.

- [13] W. He, M. Sohn, R. Ma, D.J. Kang, *Nano Energy* 78(2020)105383.
- [14] X. Sun, J. Sun, T. Li, S. Zheng, C. Wang, *Nano-Micro Lett.* 11(1), 57 (2019).
- [15] Q. Wu, J. Wang, H. Jin, Y. Dong, S. Huo, S. Yang, X. Su, B. Zhang, *Compos. Sci. Technol.*, 195 (2020) 108206.
- [16] Y. Liu, D. He, O. Dubrunfaut, A. Zhang, H. Zhang, L. Pichon, J. Bai, *Compos. Sci. Technol.*, 200 (2020)108450.
- [17] Y. Kou, X. Cheng, C.W. Macosko, *Macromolecules* 52 (2019) 7625–7637.
- [18] Gopal, K P Kandesar, N Velhal, V Phadtrare, A jatrakar, S.. Sinde, D Y. Kim, V Puri, *Chemical Engineering Journal*, 355(2019) 196-207.
- [19] H Duan, H Zhu, J Gao, D X Yan, K Dai, Y Yang, G Zhao, Y Liu Z M Li, *Journal of Materials Chemistry A*, 8 (2021) 9146-9159.
- [20] K Raagulan, B M Kim, K Y Chai, *Nanomaterials*, 10 (2020) 702 pp 22.
- [21] A M Mazrouaa, N A Mansour, M Y albe, M a oussi, M A Shenashen, M D R Awual, *Journal of Environmental Chemical Engineering*, 7 (2019) 103002
- [22] Y Liu, J Zeng, D Han, K Wu, B Yu, S Chai, F Chen, Q Fu, *Carbon*, 133 (2018) 435445.
- [23] Yunchen Du, W Liu, R Qiang, Y Wang, X Han, J Ma, P Xu, *ACS Appl Mater Interfaces* 6 (2014) 15.
- [24] D Tan, C Jiang, Q Li, S Bi, X Wang, J Song, *Journal of materials science: Materials in Electronics*, (2021) <https://doi.org/10.1007/s10854-021-05409-4>
- [25] Parveen Saini, Manju Arora, *New Polymers for Special Applications*, Chapter 3, Intech Open, 2012.
- [26] Y Li, J Wang, H Li, B Zhang, Y Cui, J Cai, Y Wang, Y Zhang, Z Bao Y Zhang, Y Wu, *Journal of Alloys and Compounds*, 821 (2020) 153531.
- [27] X. Wu, B. Han, H. Zhang, X. Xie, T. Tu, *Chem. Eng. J.* 381, 122622 (2020).

- [28] J.N. Ni, R.Y. Zhan, J. Qiu, J.C. Fan, B.B. Dong, J. Mater. Chem. C 8(34), 11748–11759 (2020).
- [29] V. T. Nguyen, B.K. Min, Y. Yi, S.J. Kim, C.-G. Choi, Chem. Eng. J. 393, 124608 (2020).
- [30] Maruti N, Muhammad Faisal, Narasimha Raghavendra, Synthetic Metals 272(2021)116664.
- [31] Sukanta Das, Sushant Sharma, Tomohiro Yokosuka, Sanjay Dhakate, Composite Structures 261 (2021) 113293.
- [32] Xichen Jia, Bin Shen, Lihua Zhang, Wenge Zheng, Carbon 173 (2021) 932e940
- [33] Xichen Jia, Bin Shen, Lihua Zhang, Wenge Zhenga Xichen Jia, Bin Shen, Lihua Zhang, Wenge Zheng, Chemical Engineering Journal 405 (2021) 126927
- [34] Robert Moučka, Michal Sedláčik, Jan Prokeš, Hayk Kasparyan, Stanislav Valtera, Dušan Kopecký, Synthetic Metals 269 (2020) 116573.
- [35] Wei Liu, Tingting Yao, Kun Jia, Jianyu Gu, Donghong Wang, and Xuehong Wei, J Mater Sci: Mater Electron (2021) 32:4393–4403.
- [36] Zhihui Zeng, Fuze Jiang, Yang Yue, Daxin Han, Luchan Lin, Shanyu Zhao, Yi-Bo Zhao, Zhengyuan Pan, Congju Li, Gustav Nyström, and Jing Wang, Adv. Mater. (2020), 1908496.
- [37] Zhihui Zeng, Fuze Jiang, Yang Yue, Daxin Han, Luchan Lin, Shanyu Zhao, Yi-Bo Zhao, Zhengyuan Pan, Congju Li, Gustav Nyström, and Jing Wang, Adv. Mater. (2020), 1908496
- [38] Deyan Kong, Jie Li, Anru Guo, Xinli Xiao, Chem Eng J 408 (2021) 127365.
- [39] Weiwei Gao, Nifang Zhao, Tian Yu, Jiabin Xi, Anran Mao, Mengqi Yuan, Hao Bai, Chao Gao, Carbon 157(2020) 570-577.
- [40] S. Uzun, M. Han, C.J. Strobel, K. Hantanasirisakul, A. Goad, G. Dion, Y. Gogotsi, Carbon, 174 (2021) 382-389.
- [41] Ping Song, Bei Liu, Chaobo Liang, Kunpeng Ruan, Hua Qiu, Zhonglei Ma, Yongqiang Guo, Junwei Gu, Nano Micor letters, 13 (2021) 91.

- [42] Yan-Jun Wana,, Xing-Miao Lia, Peng-Li Zhua,, Rong Suna,, Ching-Ping Wong, Wei-Hsin Liao, Composites Part A 130 (2020) 105764
- [43] Chaobo Liang a,1, Yuxuan Liu b,1, Yifeng Ruan a, Hua Qiu a,d,\* , Ping Song a, Jie Kong a, Haobin Zhang c, Junwei Gu, Composites: Part A 139 (2020) 106143
- [44] Priyanka Rani<sup>1</sup>, M. Basheer Ahamed<sup>1</sup>, Kalim Deshmukh, Structural, dielectric and EMS properties of polyvinyl alcohol/chitosan blend nanocomposites integrated with graphite oxide and nickel oxide nanofillers, J Mater Sci: Mater Electron 32 (2021)764–779.
- [45] Muhammad Fayzan Shakir,Iqra Abdul Rashid, Asra Tariq, Yasir Nawab, Ayesha Afzal, Muhammad Nabeel, Ahmad Naseem,Usama Hamid, EMS Characteristics of Electrically Conductive Polymer Blends of PS/PANI in Microwave and IR Region, Journal of ELECTRONIC MATERIALS, 49, (2020) 1660-1665.
- [46] Khadija Zubair , Ahmad Ashraf, Haseeb Gulzar,MFayzan Shakir , Yasir Nawab, ZAREhan and Iqra Abdul Rashid, Nano Express 2 (2021) 010038.
- [47] Wan-Cheng Yua, Ting Wanga, Ya-Hui Liua, Zhi-Guo Wanga, Ling Xua, Jian-Hua Tangb, Kun Daic, Hong-Ji Duand, Jia-Zhuang Xua, Zhong-Ming Lia, Chemical Engineering Journal 393 (2020) 124644.
- [48] Asif Raza],Amara Nasir, Mehwish Tahi, Shaista Taimur. Tariq Yasin, Muhammad Nadeem, J Appl Polym Sci. 138 (2020) 49680.
- [49] Xiaomei Wu , Bianying Wen, Composites Science and Technology 199 (2020) 108343.
- [50] Rajeev Kumar, D.P.Mondal,Anisha Chaudhary, Muhamed Shafeeq, Saroj Kumari, Composites Part A: Applied Science and Manufacturing 112 (2018) 475-484.
- [51] Sankaran, S., Deshmukh, K., Basheer Ahamed, M., Khadheer Pasha, S.K., Composites: Part A 114 (2018) 49-71.

- [52] H. Zhang, Z. Heng, J. Zhou, Y. Shi, Y. Chen, H. Zou, M. Liang, *Chemical Engineering Journal* 398 (2020) 125559.
- [53] D Jiang, V Murugadoss, Y Wang, J Lin, T Ding, Z Wang, Q Shao, C Wang, H Liu, N Lu, R Wei, A Subramania, Z Guo, *Polymer Reviews*, 59 (2019) 280-337.
- [54] P Fan, J Tang, S Jia, P Liu, J Yang, F Chen, Z Fei, M Zhong, *ACS Omega* 5 (2020) 7940–7949
- [55] Ying-Ming Li, Cong Deng, Ze-Yong Zhao, Lin-Xuan Han, Peng Lu, Yu-Zhong Wang, *Composites Part A* 131 (2020) 105769
- [56] K. Raagulan, R. Braveenth, B. M. Kim, K. J. Lim, S B Lee, M. Kim, K Y Chai, *RSC Adv.* 10 (2020) 1613.
- [57] Quan, X.H. Liang, G.B. Ji, Y. Cheng, W. Liu, J.N. Ma, Y.N. Zhang, D.R. Li, G.Y. Xu, *J. Alloy. Comp.* 728 (2017) 1065-1075.
- [58] Ping Song, Bei Liu, Chaobo Liang, Kunpeng Ruan, Hua Qiu, Zhonglei Ma, Yongqiang Guo, Junwei Gu, *Nano Micor letters*, 13 (2021) 91.
- [59] Xichen Jia, Bin Shen, Lihua Zhang, Wenge Zhenga Xichen Jia, Bin Shen, Lihua Zhang, Wenge Zheng, *Chemical Engineering Journal* 405 (2021) 126927.
- [60] Biao Zhao, Ruoming Wang, Yang Li, Yumei Ren, Xiao Li, Xiaoqin Guo, Rui Zhang and Chul B. Park, *J. Mater. Chem. C*, 8(2020), 7401
- [61] Houbao Liu, Renli Fu, Xinqing Su, Binyong Wu, He Wang, Yue Xu, Xuhai Liu, *Compos Commun* 23 (2021) 100593.
- [62] Robert Moučka, Michal Sedláčik, Jan Prokeš, Hayk Kasparyan, Stanislav Valtera, Dušan Kopecký, *Synthetic Metals* 269 (2020) 116573.

- [63] Xiuxiu Jin, Jianfeng Wang, Lunzhi Dai, Xiaoya Liu, Lei Li, Yanyu Yang, Yanxia Cao, Wanjie Wang, Hong Wuc, Shaoyun Guoc, Chem. Eng. J. 380 (2020) 122475.
- [64] Wei Liu, Tingting Yao, Kun Jia, Jianyu Gu, Donghong Wang, Xuehong Wei, J Mater Sci: Mater Electron 32 (2021) 4393-4403.
- [65] Weiwei Gao, Nifang Zhao, Tian Yu, Jiabin Xi, Anran Mao, Mengqui Yuan, Hao Bai, Chao Gao, Carbon, 157 (2020) 570-577.
- [66] Simge Uzun, Meikang Han, Christina J. Strobel, Kanit Hantanasirisakul, Adam Goad, Genevieve Dion, Yury Gogotsi, Carbon, 174 (2021) 382-389.
- [67] C Liang, Y Liu, Y Qiu, P Song, J. Kong, H Zhang, J Gu, Multi, Composites: Part A 139 (2020) 106143.

